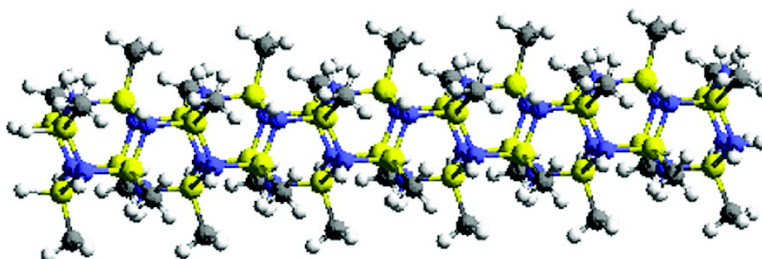


Oligomeric Rods of Alkyl- and Hydridogallium Imides

Bethany L. Kormos, Jolin A. Jegier, Paul C. Ewbank, Udo Pernisz,
Victor G. Young, Christopher J. Cramer, and Wayne L. Gladfelter

J. Am. Chem. Soc., **2005**, 127 (5), 1493-1503 • DOI: 10.1021/ja045149f • Publication Date (Web): 15 January 2005

Downloaded from <http://pubs.acs.org> on March 24, 2009



More About This Article

Additional resources and features associated with this article are available within the HTML version:

- Supporting Information
- Links to the 4 articles that cite this article, as of the time of this article download
- Access to high resolution figures
- Links to articles and content related to this article
- Copyright permission to reproduce figures and/or text from this article

[View the Full Text HTML](#)



Oligomeric Rods of Alkyl- and Hydridogallium Imides

Bethany L. Kormos,[†] Jolin A. Jegier,[†] Paul C. Ewbank,[†] Udo Pernisz,[‡]
Victor G. Young, Jr.,[†] Christopher J. Cramer,^{*,†} and Wayne L. Gladfelter^{*,†}*Contribution from the Department of Chemistry and Supercomputing Institute,
University of Minnesota, Minneapolis, Minnesota 55455, and The Dow Corning Corporation,
Midland, Michigan 48686-0994*

Received August 11, 2004; E-mail: gladfelt@chem.umn.edu, cramer@chem.umn.edu

Abstract: Reaction of $[\text{RGa}(\text{NMe}_2)_2]_2$, where R = Me, Et, Bu, and Hx, with ammonia at 150 °C in an autoclave produced insoluble white powders formulated as oligomers of $[\text{RGaNH}]_n$. The analogous reaction between NH_3 and $\text{MeGa}[\text{N}(\text{SiMe}_3)_2]_2$ at low temperature (<25 °C) formed an isolable intermediate, $[\text{MeGa}(\mu\text{-NH}_2)\text{N}(\text{SiMe}_3)_2]_2$, that was characterized using single-crystal X-ray diffraction. Infrared spectroscopy and X-ray diffraction of the oligomers were consistent with a rodlike structure comprised of six-membered, $[\text{RGaNH}]_3$ rings stacked perpendicular to the long axis of the rod. The method of synthesis, formula, and diffraction results suggested a structural similarity between the alkyl, $[\text{RGaNH}]_n$, and the previously reported hydride, $[\text{HGaNH}]_n$. The structural and electronic properties of rods having the general formula $\text{H}_3\text{-}[(\text{HXYH})_3]_n\text{-H}_3$ (XY = GaN, GeC; $n = 1\text{--}9$) were investigated using density functional theory. Atomic electronegativity differences between the group 13/15 and 14/14 systems were found to play important roles in the geometrical structures of the two rods and also caused significant differences in the electronic structures. Energetically, it was found to be increasingly favorable to add additional cyclotrigallazane rings to the GaN rods, while for the GeC rods, there was a roughly constant energy cost associated with each additional ring. The electric dipole moments of the GaN rods increased substantially with length; in the GeC rods, charge separation occurred to a much smaller extent and had a polarization opposite to that found in GaN. In addition, increased dipole moments correlated with smaller electronic excitation energies, as predicted by time-dependent density functional theory. All of the powders exhibited luminescence in the visible spectrum at room temperature. Structure observed in the photoluminescence spectra of $[\text{HGaNH}]_n$ and $[\text{MeGaNH}]_n$ was interpreted as arising from rods of different length.

Introduction

Nanoparticles of semiconductors can be synthesized in a variety of sizes and shapes, and there is much interest in correlating optical and other properties to their geometry.^{1,2} At the small end, there exist examples of well-defined clusters of sufficient size that exhibit the emergence of band properties.^{3–5} For instance, at the onset of light absorption, a series of cadmium selenide clusters ranging from 0.7 to 2 nm decrease in wavelength as the size of the cluster decreases; a feature taken as evidence of quantum confinement.⁶ We recently described a method for controlling the particle size and phase of GaN materials involving the ammonothermal conversion of $[\text{H}_2\text{-GaNH}_2]_3$ to nanocrystalline and cubic GaN.^{7,8} During the course of these investigations, we isolated imidogallane, $[\text{HGaNH}]_n$

(1), which is a stable intermediate in the ammonothermal conversion of $[\text{H}_2\text{GaNH}_2]_3$ to GaN. The conversion of $[\text{H}_2\text{-GaNH}_2]_3$ to $[\text{HGaNH}]_n$ was proposed to occur via an ammonia-assisted dehydrogenation involving several ligand redistribution and transamination/deamination reactions.⁷ The proposed structure of $[\text{HGaNH}]_n$ was that of a puckered sheet of six-membered rings in chair conformations connected by Ga–N bonds at all of the equatorial positions. Related studies of clusters, such as $[(\text{PhGa})_7(\text{NMe})_5(\text{NHMe})_4]$, formed by reaction of $[\text{RGa}(\text{NMe}_2)_2]_2$ with alkylamines, have caused us to reconsider the earlier proposed structure of $[\text{HGaNH}]_n$.^{9,10} Several of the cluster structures can be described as stacks of six-membered rings in chair conformations connected by Ga–N bonds at all of the axial positions. As suggested in earlier publications, continuation of this pattern would lead to rods (Scheme 1) of $[\text{RGaNH}]_n$ having a wurtzitic arrangement of the GaN backbone.^{9,10} Calculations by Timoshkin and Schaefer have predicted that such needle-shaped rods would be stable.¹¹

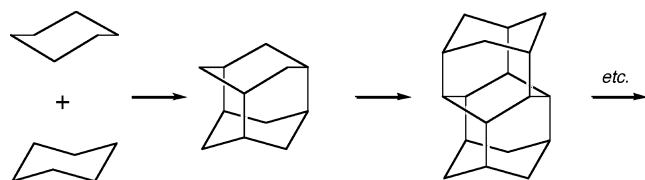
In this study, we report that ammonolysis of $[\text{RGa}(\text{NMe}_2)_2]_2$, where R = Me, Et, ⁿBu, and ⁿHx, at elevated temperatures

[†] University of Minnesota.[‡] The Dow Corning Corporation.

- (1) Trindade, T.; O'Brien, P.; Pickett, N. L. *Chem. Mater.* **2001**, *13*, 3843.
- (2) Scher, E. C.; Manna, L.; Alivisatos, A. P. *Philos. Trans. R. Soc. London, Ser. A* **2003**, *361*, 241.
- (3) Herron, N.; Calabrese, J. C.; Farneth, W. E.; Wang, Y. *Science* **1993**, *259*, 1426.
- (4) Behrens, S.; Bettenhausen, M.; Eichhofer, A.; Fenske, D. *Angew. Chem., Int. Ed.* **1998**, *36*, 2797.
- (5) Bu, X.; Zheng, N.; Li, Y.; Feng, P. *J. Am. Chem. Soc.* **2002**, *124*, 12646.
- (6) Soloviev, V. N.; Eichhoefer, A.; Fenske, D.; Banin, U. *J. Am. Chem. Soc.* **2001**, *123*, 2354.
- (7) Jegier, J. A.; McKernan, S.; Gladfelter, W. L. *Inorg. Chem.* **1999**, *38*, 2726.

(8) Jegier, J. A.; McKernan, S.; Purdy, A. P.; Gladfelter, W. L. *Chem. Mater.* **2000**, *12*, 1003.(9) Luo, B.; Gladfelter, W. L. *Inorg. Chem.* **2002**, *41*, 590.(10) Luo, B.; Gladfelter, W. L. *Inorg. Chem.* **2002**, *41*, 6249.(11) Timoshkin, A. Y.; Schaefer, H. F., III. *J. Am. Chem. Soc.* **2004**, *126*, 12141.

Scheme 1



produces a family of compounds having the formula $[\text{RGaNH}]_n$ ($\text{R} = \text{Me}$ (**2**), Et (**3**), ^nBu (**4**), and ^nHx (**5**)) and whose structures can be described as oligomeric rods. Computational analysis of their electronic structure as a function of rod length provided a basis for understanding their stability and revealed an important relationship to the dipole moment. Further insight regarding this effect was based on a comparison of the group 13/15 family of compounds, $\text{H}_3[(\text{HXYH})_3]_n\text{H}_3$ ($n = 1-9$ and $\text{XY} = \text{GaN}$), to the isoelectronic group 14/14 rods (where $\text{XY} = \text{GeC}$). Structure observed in the photoluminescence spectra of $[\text{HGaNH}]_n$ and $[\text{MeGaNH}]_n$ was interpreted as arising from rods of different length.

Experimental Section

General. All manipulations were carried out with the rigorous exclusion of oxygen and moisture using standard Schlenk and drybox techniques (Vacuum Atmospheres Company, Dri-Train Model 40-1). Diethyl ether, pentane, hexane, and toluene were distilled from sodium benzophenone ketyl immediately prior to use. Anhydrous NH_3 (Air Products) was used as received. Lithium bis(trimethylsilylamide) (Aldrich) was recrystallized from pentane. $[\text{RGa}(\text{NMe}_2)_2]_2$, where $\text{R} = \text{Me}$, Et , ^nBu , and ^nHx , was prepared using literature procedures.¹²

Infrared spectra were acquired on NaCl plates (liquids) or as KBr pellets (solids) on a Nicolet Magna-IR 560 spectrometer and are reported in cm^{-1} . Proton NMR spectra were recorded on a Varian Inova 300 spectrometer in C_6D_6 or CDCl_3 solvent and were referenced to the residual protons in the solvent (7.15 and 7.27 ppm, respectively). Melting points were obtained in sealed, nitrogen-filled capillaries and were uncorrected. Elemental analyses were obtained from Schwarzkopf Microanalytical Laboratories, Woodside, New York.

High-Pressure Experiments. Experiments involving the use of NH_3 at elevated temperatures were conducted in a steel autoclave (Parr Instrument Corporation, Model A1120HC, 50 mL capacity) equipped ethylene/propylene O-rings. The autoclave was heated using an aluminum block, and the temperature was controlled by means of an Omega temperature controller. Pressure was monitored with an Omega electronic pressure transducer.

Synthesis of $[\text{MeGaNH}]_n$ (2**). Method A:** In a drybox, the autoclave was charged with $[\text{MeGa}(\text{NMe}_2)_2]_2$ (10.12 mmol, 3.500 g) and sealed. The autoclave was then attached to the Schlenk line, cooled to -78°C , and evacuated. Ammonia (approximately 15 mL) was then condensed into the autoclave. The vessel was then sealed and heated to 150°C over the course of 30 min reaching a pressure of 8.86 MPa. The reactor was maintained at this temperature for an additional 30 min reaching a maximum pressure of 10.9 MPa. The reactor was removed from the heating block, and the ammonia was vented. The autoclave was opened in the drybox, and **2** was isolated as a white powder in essentially quantitative yield (2.018 g). Mp $>260^\circ\text{C}$. IR (KBr): 3353 w, 3291 m, 2959 m, 2926 sh, 2891 m, 1208 m, 940 s, 890 s, 704 s. Anal. Calcd for CH_4GaN : C, 12.04; H, 4.04; N, 14.04; Ga, 69.88. Found: C, 12.51; H, 4.23; N, 13.50; Ga, 69.64.

Method B: The procedure was as for **A** above using $\text{MeGa}[\text{N}(\text{SiMe}_3)_2]_2$ (4.932 mmol, 2.000 g), NH_3 (approximately 15 mL), and a reactor pressure of 9.79 MPa. The product was isolated as a sticky

off-white solid, which was dried under vacuum to give an off-white powder (0.483 g). The product was nearly identical to that produced from **A**. However, the IR spectrum indicated the presence of residual $-\text{NSi}(\text{CH}_3)_3$ groups.

Synthesis of $[\text{EtGaNH}]_n$ (3**).** The procedure was as for **2** above using $[\text{EtGa}(\text{NMe}_2)_2]_2$ (9.362 mmol, 3.500 g), NH_3 (approximately 15 mL), and a reactor pressure of 11.0 MPa. Compound **3** was isolated as a white solid in essentially quantitative yield (2.128 g). Mp $>260^\circ\text{C}$. IR (KBr): 33343 w, 3284 m, 2942 m, 2899 m, 2863 m, 2808 w, 1465 w, 1419 w, 1375 w, 1260 w, 971 s(br), 916 m. Anal. Calcd for $\text{C}_2\text{H}_6\text{GaN}$: C, 21.11; H, 5.31; N, 12.31; Ga, 61.26. Found: C, 21.32; H, 5.61; N, 11.92; Ga, 59.14.

Synthesis of $[\text{BuGaNH}]_n$ (4**).** The procedure was as for **2** above using $[\text{BuGa}(\text{NMe}_2)_2]_2$ (5.872 mmol, 2.525 g), NH_3 (approximately 15 mL), and a reactor pressure of 10.5 MPa. Compound **4** was isolated as an off-white solid in essentially quantitative yield (1.667 g). Mp $>260^\circ\text{C}$. IR (KBr): 3342 w, 3284 m, 2956 m, 2908 s(br), 2872 m, 2838 w, 2801 w, 1464 m, 1375 w, 1069 w, 958 s. Anal. Calcd for $\text{C}_4\text{H}_{10}\text{GaN}$: C, 33.87; H, 7.11; N, 9.87; Ga, 49.15. Found: C, 34.12; H, 7.17; N, 6.68; Ga, 47.97.

Synthesis of $[\text{HxGaNH}]_n$ (5**).** The procedure was as for **2** above using $[\text{HxGa}(\text{NMe}_2)_2]_2$ (6.198 mmol, 3.013 g), NH_3 (approximately 15 mL), and a reactor pressure of 7.54 MPa. Compound **5** was isolated as a waxy, off-white solid in essentially quantitative yield (2.128 g). Mp $>260^\circ\text{C}$. IR (KBr): 3341 w, 3285 m, 2955 m, 2916 s(br), 2871 m, 2845 m, 2799 w, 1466 s, 1376 m, 1154 w, 1095 m, 956 s(br), 927 sh. Anal. Calcd for $\text{C}_6\text{H}_{14}\text{GaN}$: C, 41.03; H, 8.31; N, 8.24; Ga, 41.03. Found: C, 42.27; H, 9.34; N, 7.76; Ga, 40.37. Changes in reaction time (24 h) and reactor pressure (385 psig) did not noticeably effect the properties of the product. A small amount of **5** was dissolved in refluxing hexanes, and its IR spectrum was obtained in solution. IR (hexanes): 3342 vw, 3284 w, 1261 s, 1096 s, 1021 s, 970 s, 804 s. After several hours, an IR spectrum of the solid that precipitated was taken. IR (KBr): 3284 w, 3145 w(br), 2959 m, 2917 m, 2871 m, 2847 m, 1466 m, 1261 s, 1095 s, 1021 s, 958 s, 801 s.

Synthesis of $[\text{MeGa}(\mu\text{-NH}_2)\text{N}(\text{SiMe}_3)_2]_2$ (6**).** Onto $\text{MeGa}[\text{N}(\text{SiMe}_3)_2]_2$ (4.932 mmol, 2.000 g) was condensed NH_3 (40 mL) at -196°C . The flask was warmed to -55°C , and the NH_3 was allowed to melt. The mixture was allowed to stir for several hours. During this time, the solid disappeared and was replaced with a nearly colorless oil. The mixture was stirred overnight, and the NH_3 was allowed to evaporate slowly, resulting in a crystalline solid. The solid was dissolved in pentane (25 mL), the solution filtered to remove some insoluble material, and concentrated to 6 mL. The solution was stored at -25°C for several days, resulting in the isolation of **6** as colorless blocks which were suitable for single-crystal X-ray diffraction studies (0.713 g, 55%). Mp $105-109^\circ\text{C}$. IR (KBr): 3387 s, 3318 s, 2951 s, 2897 m, 1485 m, 1261 s, 1249 s, 1201 m, 967 s, 886 m, 833 s(br). ^1H NMR (C_6D_6): δ -0.27 (s, 3H, GaCH_3), -0.08 (s, 3H, GaCH_3), 0.18 (s, 18H, $\text{N}(\text{SiMe}_3)_2$), 0.20 (s, 18H, $\text{N}(\text{SiMe}_3)_2$), 0.48 (d (br), 2H, NH_2), 1.09 (t (br), 2H, NH_2). MS (CI, isobutane): 523.1 (dimer, $\text{M}^+ + \text{H}$), 507.1 (dimer, $\text{M}^+ - \text{NH}_2$), 362.0 (dimer, $\text{M}^+ - \text{N}(\text{SiMe}_3)_2$), 245.0 (monomer, $\text{M}^+ - \text{NH}_2$). Anal. Calcd for $\text{C}_{14}\text{H}_{46}\text{Ga}_2\text{N}_4\text{Si}_4$: C, 32.62; H, 9.01; N, 10.87. Found: C, 31.29; H, 9.52; N, 10.05.

Thermolysis of $[\text{MeGa}(\mu\text{-NH}_2)\text{N}(\text{SiMe}_3)_2]_2$. A sample of **6** (150 mg) was slowly heated. The sample melted at 110°C and began to evolve gas at approximately 170°C . The temperature was increased to 185°C and held for 45 min. During this time, the sample slowly solidified, forming a colorless glass. After cooling, approximately 25 mg of the glassy product was recovered. IR spectroscopy showed it to be similar but not identical to **2**. IR (KBr): 3352 m, 3294 m, 2953 s, 2897 m, 1511 m, 1249 s, 1211 s, 941 s(br), 886 s, 833 s, 707 s.

X-ray Diffraction Studies. Powder XRD data were collected on a Siemens D5005 diffractometer using monochromatic (graphite) $\text{Cu K}\alpha$ radiation. Samples were ground in a mortar and pestle and dispersed on glass slides. Crystal structure modeling was conducted using Cerius2.

(12) Jegier, J. A.; Luo, B.; Buss, C. E.; Gladfelter, W. L. *Inorg. Chem.* **2001**, *40*, 6017.

Table 1. Crystallographic Data for **6**

chemical formula	C ₇ H ₂₃ GaN ₂ Si ₂ 6
formula weight	261.17
space group	P2 ₁ /n
a, Å	6.7657(3)
b, Å	16.3874(7)
c, Å	12.2285(5)
β, deg	90.023(1)
V, Å ³	1355.8(1)
Z	4
T, °C	−100
λ, Å	0.71073
ρ _{calc} , g cm ^{−3}	1.280
μ, cm ^{−1}	21.70
R ₁ , wR ₂ ^a [I > 2σ(I)]	0.0307, 0.0700

^a R₁ = Σ||F_o| − |F_c||/Σ|F_o| and wR₂ = {Σ[w(F_o² − F_c²)²]/Σ[w(F_o²)²]}^{1/2}, where w = q/σ²(F_o²) + (aP)² + (bP), P = (F_o² + 2F_c²)/3, and a and b are constants given in Supporting Information.

Graph S1 in the Supporting Information compares a calculated and experimental diffraction pattern for **3**.

A suitable crystal of **6** was attached to a glass fiber under a nitrogen atmosphere and mounted on a Siemens SMART Platform. Data were collected at 173 K, and the final cell constants were calculated from a set of 4556 strong reflections. The space group P2₁/n was determined based upon systematic absences and intensity statistics. A successful direct-methods solution was applied to both structures that provided most non-hydrogen atoms from the E-maps. Several full-matrix, least squares/difference Fourier cycles were performed, which located the remainder of the non-hydrogen atoms. All hydrogen atoms were placed in ideal positions and refined as riding atoms with individual isotropic displacement parameters. All calculations were performed using SGI INDY R4400-SC or Pentium computers using the SHELXTL V5.0 suite of programs. The experimental conditions and unit cell information are summarized in Table 1.

Photoluminescence Studies. Solid samples of **1** and **2** were loaded into a quartz cuvette in a nitrogen-filled glovebox and sealed. Front-face fluorescence measurements were acquired with a Spex F212 spectrofluorometer using a xenon source as previously described.¹³

Computational Methods. All calculations made use of the hybrid functional B3LYP^{14,15} which combines¹⁶ exact Hartree–Fock exchange with the gradient-corrected exchange functional of Becke¹⁷ and the gradient-corrected correlation functional of Lee, Yang, and Parr.¹⁵ This functional has previously been shown to provide good performance in the computation of structures and energies for monomers and dimers of group 13/15 species, including gallazanes.^{18,19} Computational studies of organogallium amido and imido clusters using related theoretical methods have been reported.^{11,20}

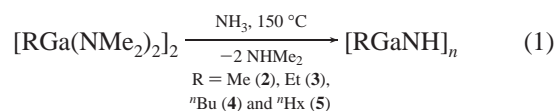
Geometry optimizations were carried out using three different basis set combinations; practical limitations restricted the optimization of the longest rods to using only the most economical basis. Our best basis, which we denote hereafter as CEP*, is defined as follows: CEP-31G basis^{21–23} and 28-electron effective core potential (ECP) on Ge augmented with a single set of d functions having exponent 0.2; CEP-31G basis and 10-electron ECP on Ga (the looser split valence 3d functions in this instance can serve as polarization functions); CEP-

31G(d) basis and 2-electron ECPs on N and C; 3-21G basis²⁴ on H. Our next best basis, which we denote as CEP, removes the polarization functions from Ge, N, and C but is otherwise equivalent to CEP*. Finally, our smallest basis set/ECP combination, hereafter called MB, employs the Hay–Wadt^{25,26} minimal basis and 28-electron ECPs for Ga and Ge and the STO-3G basis set²⁴ for N, C, and H. All optimized geometries were confirmed as minima by computation of analytic second derivatives.¹⁶

Energies reported below correspond to single-point B3LYP/CEP*/B3LYP/MB calculations. Excited-state energies for the first three states above the ground state were computed by time-dependent density functional theory (TDDFT)^{27–29} for all rods at the B3LYP/CEP*/B3LYP/MB level, as well. All calculations were performed using Gaussian 98, revision A.11.³⁰

Results

Synthesis of Alkylgallium Imides. Compounds **2–5** were synthesized using ammonothermal techniques (eq 1) in nearly quantitative yield and isolated as white to off-white solids (**5** was isolated as a yellowish, waxy solid).



Changes in reaction time (30 min to 24 h) and reactor pressure (5.5–11.7 MPa) had little or no effect on the properties of the product. The use of related alkylgallium amide precursors of the general formula RGa[N(SiMe₃)₂]₂ also resulted in nearly quantitative yields of alkylgallium imides. These precursors, however, resulted in impure samples; the IR spectra indicated the presence of residual −NSi(CH₃)₂ groups. Carbon, hydrogen, nitrogen, and gallium analyses were satisfactory for **2**, but showed small deviations from ideality in compounds **3** and **5**. In **4**, both N and Ga analyses were lower than expected. These deviations may be due to the formation of GaN in the analytical procedure.

Like imidogallane, [HGaNH]_n, **2–5** were found to be insoluble in nearly all solvents except for strong mineral acids with which they reacted. The hexyl derivative, **5**, did exhibit some apparent solubility in refluxing solvents, such as hexane, toluene, and chloroform, but the infrared spectrum of the powder formed by evaporation of the solvent was not identical to the starting powder.

The IR spectra of **2–5**, obtained as KBr pellets, exhibited similar features and possessed ν_{N–H} and ω,τ_{N–H} vibrational modes consistent with those of an imide N–H moiety. The ν_{N–H}

(13) Guenoun, P.; Lipsky, S.; Mays, J. W.; Tirrell, M. *Langmuir* **1996**, *12*, 1425.

(14) Becke, A. D. *J. Chem. Phys.* **1993**, *98*, 5648.

(15) Lee, C.; Yang, W.; Parr, R. G. *Phys. Rev. B: Condens. Matter* **1988**, *37*, 785.

(16) Hehre, W. J.; Stewart, R. F.; Pople, J. A. *J. Chem. Phys.* **1969**, *51*, 2657.

(17) Becke, A. D. *Phys. Rev. A* **1988**, *38*, 3098.

(18) Cramer, C. J.; Gladfelter, W. L. *Inorg. Chem.* **1997**, *36*, 5358.

(19) Campbell, J. P.; Hwang, J.-W.; Young, V. G., Jr.; Von Dreele, R. B.; Cramer, C. J.; Gladfelter, W. L. *J. Am. Chem. Soc.* **1998**, *120*, 521.

(20) Timoshkin, A. Y.; Bettinger, H. F.; Schaefer, H. F., III. *J. Phys. Chem. A* **2001**, *105*, 3249.

(21) Stevens, W. J.; Basch, H.; Krauss, J. *J. Chem. Phys.* **1984**, *81*, 6026.

(22) Stevens, W. J.; Krauss, M.; Basch, H.; Jasien, P. G. *Can. J. Chem.* **1992**, *70*, 612.

(23) Cundari, T. R.; Stevens, W. J. *J. Chem. Phys.* **1993**, *98*, 5555.

(24) Hay, P. J.; Wadt, W. R. *J. Chem. Phys.* **1985**, *82*, 270.

(25) Wadt, W. R.; Hay, P. J. *J. Chem. Phys.* **1985**, *82*, 284.

(26) Hay, P. J.; Wadt, W. R. *J. Chem. Phys.* **1985**, *82*, 299.

(27) Stratmann, R. E.; Scuseria, G. E.; Frisch, M. J. *J. Chem. Phys.* **1998**, *109*, 8218.

(28) Bauernschmitt, R.; Ahlrichs, R. *Chem. Phys. Lett.* **1996**, *256*, 454.

(29) Casida, M. E.; Jamorski, C.; Casida, K. C.; Salahub, D. R. *J. Chem. Phys.* **1998**, *108*, 4439.

(30) Frisch, M. J.; Trucks, G. W.; Schlegel, H. B.; Scuseria, G. E.; Robb, M. A.; Cheeseman, J. R.; Zakrzewski, V. G.; Montgomery, J. A., Jr.; Stratmann, R. E.; Burant, J. C.; Dapprich, S.; Millam, J. M.; Daniels, A. D.; Kudin, K. N.; Strain, M. C.; Farkas, O.; Tomasi, J.; Barone, V.; Cossi, M.; Cammi, R.; Mennucci, B.; Pomelli, C.; Adamo, C.; Clifford, S.; Ochterski, J.; Petersson, G. A.; Ayala, P. Y.; Cui, Q.; Morokuma, K.; Malick, D. K.; Rabuck, A. D.; Raghavachari, K.; Foresman, J. B.; Cioslowski, J.; Ortiz, J. V.; Stefanov, B. B.; Liu, G.; Liashenko, A.; Piskorz, P.; Komaromi, I.; Gomperts, R.; Martin, R. L.; Fox, D. J.; Keith, T.; Al-Laham, M. A.; Peng, C. Y.; Nanayakkara, A.; Gonzalez, C.; Challacombe, M.; Gill, P. M. W.; Johnson, B. G.; Chen, W.; Wong, M. W.; Andres, J. L.; Head-Gordon, M.; Replogle, E. S.; Pople, J. A. *Gaussian 98*, revision A.11; Gaussian, Inc.: Pittsburgh, PA, 1998.

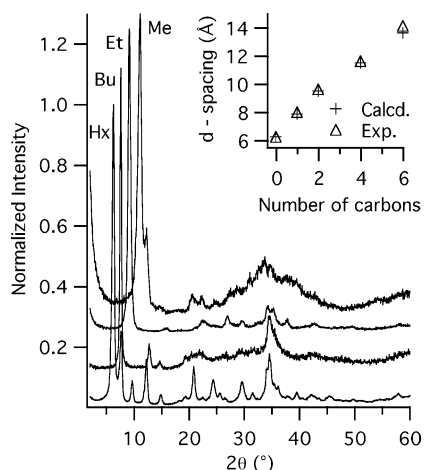


Figure 1. X-ray diffraction patterns of $[\text{MeGaNH}]_n$ **2**, $[\text{EtGaNH}]_n$ **3**, $[\text{BuGaNH}]_n$ **4**, and $[\text{HxGaNH}]_n$ **5**. The inset graph shows a comparison of experimental and calculated d spacings for the (110) reflection for compounds **1–5**.

modes for **2–5** were observed as a set of two peaks, a medium intensity peak ranging from 3284 (**5**) to 3291 cm^{-1} (**2**) and a very weak intensity peak ranging from 3334 (**5**) to 3353 cm^{-1} (**2**). The $\omega, \tau_{\text{N-H}}$ modes for **2–5** were also observed as a set of two peaks ranging from 890 and 940 cm^{-1} for **2** to 916 and 971 cm^{-1} for **3**. These N–H modes were nearly identical to those found for the parent poly(imidogallane), $[\text{HGaNH}]_n$ ($\nu_{\text{N-H}}$ 3280, $\omega, \tau_{\text{N-H}}$ 962, 906), and suggested that **2–5** were isostructural with $[\text{HGaNH}]_n$.⁸ The IR spectrum of **5** underwent significant changes upon attempted dissolution in refluxing hexanes. While the solution phase spectrum exhibited essentially no change in $\nu_{\text{N-H}}$, new peaks appeared at 1261, 1096, 1021, and 804 cm^{-1} . The solid that precipitated from this solution also appeared different from that of as-prepared **5**. The IR spectrum (KBr) of this solid was very similar to that of **5** in solution with the exception of a new peak that was attributed to $\nu_{\text{N-H}}$ at 3145 cm^{-1} .

X-ray Powder Diffraction. The X-ray powder diffraction patterns (Figure 1) of **2–5** were dominated by one very intense diffraction peak at high d spacing. For **2–4**, broad, less intense peaks appeared at lower d spacings, whereas the hexyl derivative (**5**) exhibited narrower, though still less intense reflections. The improved signal-to-noise ratio apparent in Figure 1 for **5** was due to a longer data collection time. The most intense diffraction peak in all of these diffraction patterns was shifted to higher d spacing (from 7.96 Å for **2** to 13.85 Å for **5**) as the size of the gallium substituent increased. These values are all greater than that found for $[\text{HGaNH}]_n$ (6.30 Å).⁸

Models of compounds **1–5** generated using Cerius2 were used to estimate the packing of rods for comparison to the diffraction results. The model rods consisted of 12 $[\text{RGaNH}]_3$ rings capped with three hydrogens on each end. Although simulations in Cerius2 were not as accurate as the calculations described below (the Ga–N bond distances were underestimated by approximately 0.2 Å), this was expected to have minimal impact on how the rods packed. On the basis of the hexagonal crystal system assignment for the structure of $[\text{HGaNH}]_n$, the expectation that long rods of uniform diameter would pack in a hexagonal motif, and the 3-fold rotational symmetry of individual rods, we chose to minimize structures in trigonal space groups. As a test of this decision, minimization of the

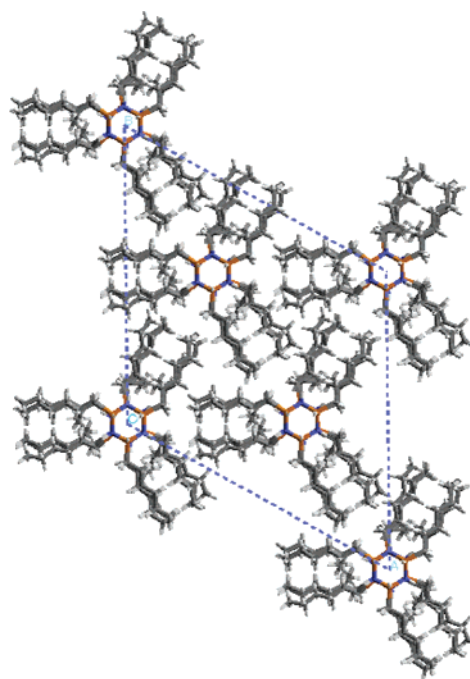


Figure 2. View down c axis showing the packing of $\text{H}_3[(\text{HxGaNH})_3]_{12}\text{H}_3$ in space group $R3$.

crystal structure of $\text{H}_3[(\text{HxGaNH})_3]_{12}\text{H}_3$ was also carried out in the triclinic space group $P1$. Although the hexyl side chains were not as well ordered in the converged structure, the final packing arrangement exhibited the same hexagonal motif and a similar inter-rod distance as that found in the trigonal space groups. Specific assignment of the space group within the trigonal crystal system also had little impact on rod packing and inter-rod distance in the a – b plane. Inclusion of an inversion center ($P3$ vs $P\bar{3}$) also had no significant impact on these factors. The distances compared in the inset graph of Figure 1 showed excellent agreement between the experimental and calculated d spacing for the (110) reflection. The calculated d spacings were derived for structures **2–5** modeled in $R3$ with the rod lying on a 3-fold axis. Unlike **2–5**, compound **1** (modeled in $P3$) exhibited a large reflection at a lower value of 2θ assigned to (001), which would be systematically absent in $R3$. Attempts to find similar reflections in **2–5** using small angle measurements were unsuccessful. The flexible Et, Bu, and Hx chains in **3–5** assemble on three edges of each rod and interlock with neighboring chains in a gearlike fashion (Figure 2).

Photoluminescence. Room-temperature photoluminescence spectra of $[\text{HGaNH}]_n$ and $[\text{MeGaNH}]_n$ powders are shown in Figures 3 and 4, respectively. The figures indicate that both samples absorbed in the ultraviolet range and emitted toward the blue end of the visible spectrum. The emission spectrum for $[\text{HGaNH}]_n$ exhibited structure with at least three distinct maxima at 409, 429, and 455 nm. Exposing the powder of $[\text{HGaNH}]_n$ to air for one week caused a reduction of emission intensity, but the reduction was not uniform over the spectrum; the maxima at 429 and 455 nm decreased relative to the one at 409 nm. Longer-term exposure of all compounds resulted in decomposition and loss of all emission.

Emission from $[\text{MeGaNH}]_n$ occurred in the same spectral region as that of **1**; however, the intensity was over an order of magnitude greater. The spectra displayed more distinct structure than observed in **1**, with a particularly intense emission observed

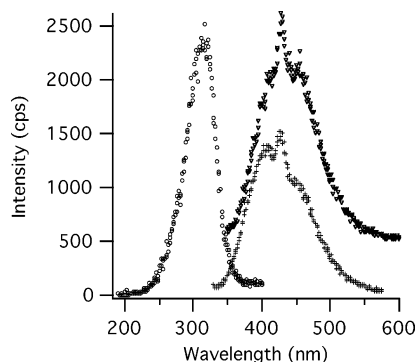


Figure 3. Room-temperature photoluminescence spectra of $[\text{HGaNH}]_n$ powder: (▼) emission spectrum with $\lambda_{\text{ex}} = 320$ nm (data offset by 500 cps); (+) emission spectrum with $\lambda_{\text{ex}} = 320$ nm (sample exposed to air for one week); (○) excitation spectrum with $\lambda_{\text{obs}} = 430$ nm.

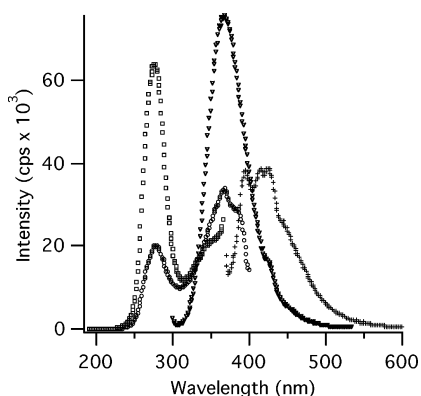
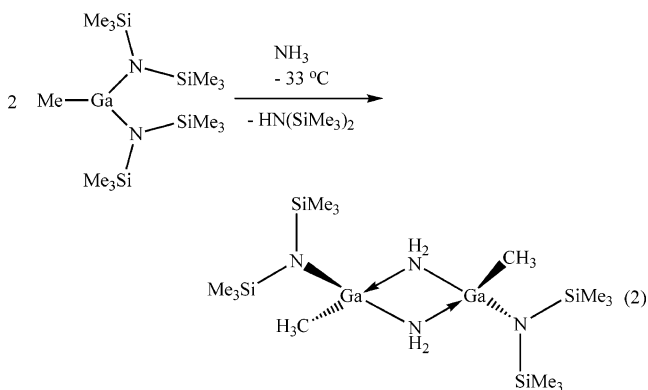


Figure 4. Room-temperature photoluminescence spectra of $[\text{MeGaNH}]_n$ powder: (▼) emission spectrum with $\lambda_{\text{ex}} = 275$ nm (intensity scaled by 0.5); (+) emission spectrum with $\lambda_{\text{ex}} = 345$ nm; (□) excitation spectrum with $\lambda_{\text{obs}} = 390$ nm (intensity scaled by 0.5); (○) excitation spectrum with $\lambda_{\text{obs}} = 425$ nm (intensity scaled by 0.5).

at 369 nm and less intense emission maxima found at 399, 429, and 460 nm. The relative intensities were dependent on the excitation wavelength. The excitation spectra indicated that the emission maximum at 369 nm resulted from an intense absorption at 275 nm. The longer wavelength emission peaks resulted from absorption in the range of 300–400 nm.

Isolation of an Intermediate in the Transamination Reaction. The effect of reaction temperature on the transamination/deamination process was also studied by reacting $\text{MeGa}[\text{N}(\text{SiMe}_3)_2]$ with NH_3 at -33 °C (eq 2).



Removal of the volatiles did not result in **2**, but rather a colorless polycrystalline solid, **6**, that was recrystallized from pentane and isolated in 55% yield. Peaks at 3387 and 3318 cm^{-1}

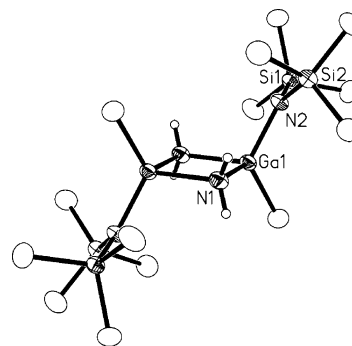


Figure 5. Molecular structure and atom-labeling scheme for $[\text{MeGa}(\mu\text{-NH}_2)\text{N}(\text{SiMe}_3)_2]_2$ **6**. All non-hydrogen atoms are shown at the 50% probability level.

Table 2. Selected Bond Lengths (Å) and Angles (deg) for **6**

$\text{C}_7\text{H}_{23}\text{Ga}_2\text{N}_2\text{Si}_2$ 6			
Ga1–C1	1.957(3)	Ga1–N2	1.889(2)
Ga1–N1	1.995(2)	Ga1–N1A	2.004(2)
N2–Ga1–C1	121.43(12)	N1–Ga1–N1A	85.45(9)
Ga1–N1–Ga1A	94.55(9)	N1–Ga1–N2	112.41(9)
N1–Ga1–C1	108.85(12)	N1A–Ga1–C1	113.17(12)

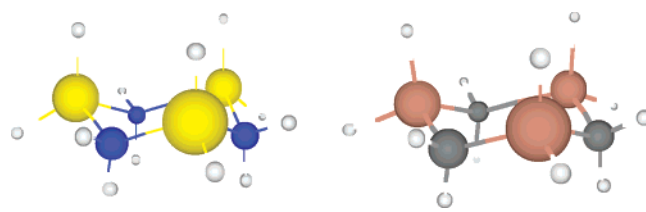
in the IR spectrum of **6** indicated the presence of NH_2 groups, while resonances at 0.18 and 0.12 ppm in the ^1H NMR spectrum indicated the presence of NSiMe_3 moieties. The presence of both NH_2 and NSiMe_3 groups led us to conclude that **6** was $[\text{MeGa}(\mu\text{-NH}_2)\text{N}(\text{SiMe}_3)_2]_2$. The presence of two sets of NSiMe_3 and GaMe resonances (-0.08 and -0.27 ppm) in a 70:30 ratio suggested a dimeric structure and cis/trans isomerism similar to that seen in $[\text{RGa}(\text{NMe}_2)_2]_2$. The mass spectrum confirmed the dimeric nature of **6** in the gas phase with peaks at 523, 507, and 362 m/e being attributed to $(\text{dimer} + \text{H})^+$, $(\text{dimer} - \text{NH}_2)^+$, and $(\text{dimer} - \text{N}(\text{SiMe}_3)_2)^+$, respectively. Additionally, a peak at 245 was observed, which could be attributed to $(\text{monomer} - \text{NH}_2)^+$.

The molecular structure of **6** is shown in Figure 5, and relevant bond lengths and angles are listed in Table 2. In the solid state, **6** was found to be dimeric with one-half of the molecule in the asymmetric unit and the other half generated through an inversion center. The dimer features a Ga_2N_2 core with bridging NH_2 (N1, N1a) groups and terminal NSiMe_3 (N2, N2a) moieties. As dictated by symmetry, N2 and N2a are anti with respect to one another, which results in a trans arrangement around the Ga_2N_2 core. This is a common dimer geometry, and the bond lengths and angles are unexceptional.³¹

Computational Results and Comparisons to Known Structures. Chair structures (C_{3v}) for the parent cyclotrigallazane and 1,3,5-trigermacyclohexane rings ($\text{H}_3[(\text{HXYH})_3]_n\text{H}_3$, $n = 1$) were optimized at the B3LYP/CEP*, B3LYP/CEP, and B3LYP/MB levels. Key computed structural parameters are compared to those from X-ray diffraction studies^{19,32} in Table 3 (for the figures in Table 3 and all figures in this paper, Ge atoms are bronze, Ga atoms golden, N atoms blue, C atoms gray, and H atoms white). With the largest basis set CEP*, the computed values were in fairly good agreement with the experimental ones. There was a tendency for the theoretical model to overestimate the heavy-atom–heavy-atom bond length and also the valence

(31) Carmalt, C. J. *Coord. Chem. Rev.* **2001**, 223, 217.

(32) Schmidbauer, H.; Rott, J.; Reber, G.; Mueller, G. Z. *Naturforsch., B: Chem. Sci.* **1988**, 43, 727.

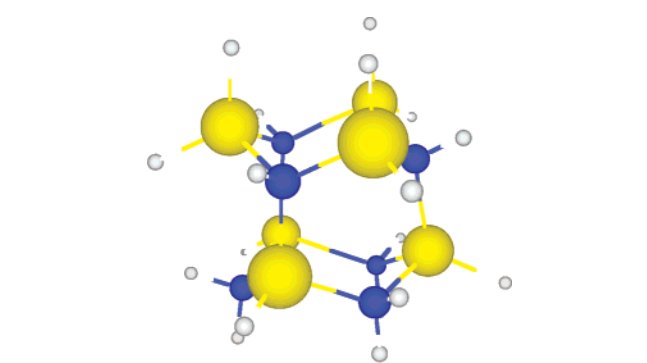
Table 3. Computed B3LYP Heavy-Atom Bond Lengths (Å) and Angles (deg) Compared to X-ray Diffraction Structures of Cyclotrigallazane and 1,3,5-Trigermacyclohexane


	Basis			exp ^a
	MB	CEP	CEP*	
Ga1–N2 ^b	1.994	2.020	2.030	1.987
N2–Ga3				1.972
Ga3–N4				1.975
Ga1–N2–Ga3	124.6	120.9	119.4	116.9
Ga3–N4–Ga5				117.3
N2–Ga3–N4	106.8	105.0	99.8	100.6
N2–Ga1–N6				99.9
Ge1–C2	2.035	1.975	1.975	1.955
C2–Ge3				1.944
Ge3–C4				1.953
Ge1–C2–Ge3	113.41	114.0	113.6	112.7
Ge3–C4–Ge5				111.2
C2–Ge3–C4	111.7	111.0	110.1	110.0
C2–Ge1–C6				109.5

^a Cyclotrigallazane data from ref 19, and 1,3,5-trigermacyclohexane data from ref 32. ^b Computed data refer to structures having C_{3v} symmetry and include only unique bond lengths and angles; experimental crystal structures include multiple measurements because of lower unit cell symmetry.

angle at nitrogen in the cyclotrigallazane. The removal of polarization functions from the CEP* basis set did not seem to have much effect on the computed 1,3,5-trigermacyclohexane structure, but it caused some flattening of the cyclotrigallazane ring, as evidenced by the 1–5° larger valence bond angles at both Ga and N. Finally, at the B3LYP/MB level, some cancellation of errors rendered the Ga–N bond length more accurate in cyclotrigallazane, while the bond angles become less so. For 1,3,5-trigermacyclohexane, the error in bond length increased with the smaller basis set, while the bond angles remained reasonably well predicted.

Additional geometric comparisons were made to the crystal structures for two substituted compounds analogous to our $n = 2$ rods, namely, $[\text{PhGaNMe}]_7$ ⁹ and $[(\text{PhGa})_7(\text{NHMe})_4(\text{NMe})_5]$.¹⁰ The $[\text{PhGaNMe}]_7$ structure corresponded exactly to the $n = 2$ rod, except that the Ga and N atoms bear phenyl substituents instead of H atoms, and GaPh and NPh moieties capped the free nitrogen and gallium ends of the rod, respectively. The $[(\text{PhGa})_7(\text{NHMe})_4(\text{NMe})_5]$ structure had the same core, but was capped by a substituted GaN_3 substituent, creating an adamantane-like structure. This latter structure included a nonquaternized nitrogen atom in one ring of the rod. Comparisons between these structures and the theoretical $\text{H}_3[(\text{HXYH})_3]_n\text{H}_3$ $n = 2$ rod computed at the B3LYP/CEP and B3LYP/MB levels are provided in Table 4. The agreement between theory and experiment was reasonably good, better than for the isolated ring monomers discussed above, particularly for the Ga–N bond lengths. The accuracy of the predictions for the Ga–N_{||} bonds, which was expected to be least perturbed by the substitutions, was particularly encouraging. Bond angles were also predicted fairly well, with the exception of the valence angles for the atoms capped by the PhGa and PhN groups in $[\text{PhGaNMe}]_7$, which were highly distorted by the single atom connection

Table 4. Computed B3LYP Heavy-Atom Bond Lengths (Å) and Angles (deg) for $\text{H}_3[(\text{HXYH})_3]_2\text{H}_3$ Compared to Experimental X-ray Diffraction Structures of $[\text{PhGaNMe}]_7$ and $[(\text{PhGa})_7(\text{NHMe})_4(\text{NMe})_5]$


	Basis		exp ^a [PhGaNMe] ₇	exp ^b [(PhGa) ₇ (NHMe) ₄ (NMe) ₅]
	MB	CEP		
Ga–N	2.008 ^c	2.017	1.968–1.986	1.906–1.998
	1.994	2.012	1.968–1.999	1.957–1.984
Ga–N ^d	1.936	1.929	1.932–1.956	1.961–1.988
Ga–N–Ga	112.8	114.1	89.5–91.0	112.9–114.0
	118.3	117.3	118.5–119.3	114.9–119.1
N–Ga–N	99.8	101.7	108.7–111.3	104.9–107.7
	101.6	102.2	88.7–89.5	104.6–105.6

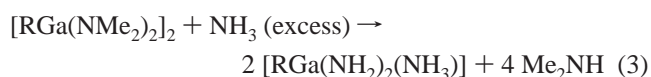
^a From ref 9. ^b From ref 10. ^c Upper number refers to upper ring, lower number refers to lower ring. Computed data refer to structures having C_{3v} symmetry and include only unique bond lengths and angles; experimental crystal structures include multiple measurements because of lower unit cell symmetry. ^d Ga–N_{||} indicates the three Ga–N bonds that are parallel to the rod axis.

among them and thus did not provide a relevant comparison in any case. It is possible that the rods described in this paper are capped in the same fashion as those observed in $[\text{PhGaNMe}]_7$ or $[(\text{PhGa})_7(\text{N}^i\text{Bu})_4(\text{NH}^i\text{Bu})_5]$. Even for rods with a relatively small length, elemental analysis could not easily differentiate the formulas of $\text{H}_3(\text{RGaNH})_n\text{H}_3$, $\text{HN}(\text{RGaNH})_n\text{GaR}$, and $\text{H}_2(\text{RGaNH})_n[\text{RGa}(\text{NH})(\text{NH}_2)_2]$.

The utility of the MB basis set evidently improved on going from the parent ring to the rod of two rings, although some errors remained. Given that practical limitations restricted us to the use of the MB basis set for the largest rods, and given that we wanted to make comparisons of all rods at a consistent level, and finally given the generally good performance of the B3LYP/MB model for the data in Table 4, we considered the geometrical errors implicit in the use of the MB basis to be acceptably small. We note that we were in any case more interested in trends as a function of rod growth than we were in absolute structures of the rods, and to the extent our results were interpreted primarily in that vein, errors should be still further reduced.

Discussion

The reaction of $[\text{RGa}(\text{NMe}_2)_2]_2$ in liquid or supercritical NH_3 was expected to lead initially to scission of the dimeric structure and substitution of the dimethylamido ligands (eq 3).



At lower reaction temperatures, use of the sterically bulky $-\text{N}(\text{SiMe}_3)_2$ ligand in place of the dimethylamido ligand

allowed isolation of the monosubstituted intermediate, [RGa-(μ -NH₂)N(SiMe₃)₂]₂. Observation that the organogallium moiety remained intact under these conditions was consistent with the known robust nature of the single Ga–C bond in compounds having the formula RGaX₂, where X is an electronegative ligand (e.g., OH), and with the low acidity of NH₃. In analogy to the step proposed in the formation of [HGaNH]_n both from [H₂-GaNH₂]₃⁷ and [HGa(NH₂)₂]₂,³³ eq 4 showed loss of 2 equiv of ammonia.



We had no evidence to support a mechanism for this reaction, nor could we confirm that [RGaNH] monomers were the growth species in forming the oligomers. It seemed likely that under the conditions of the reaction, loss of ammonia from [RGa-(NH₂)₂(NH₃)] may be one part of a complex set of equilibria involving the solvent and the growing oligomer. The consistent elemental analytical results, the similar luminescent behavior, and the similarities in the IR spectroscopy all suggested a similar structure for this family of materials. Unfortunately, their insolubility thwarted attempts to measure solution spectroscopic properties and to separate oligomers of differing length.

Although single-crystal X-ray crystallographic analysis was not possible, sufficient order was present in the powders to diffract X-rays, and for each compound, the powder pattern was dominated by a large reflection at low angle and weaker reflections at higher angles (Figure 1). These diffraction patterns were similar to that observed for [HGaNH]_n. On the basis of XRD and electron diffraction results, a hexagonal symmetry was assigned to [HGaNH]_n, but the disparity between the experimental lattice constants and the proposed 2-D sheet structure was not reconciled satisfactorily.⁷ Reassigning the structure to rods consisting of chair-shaped, six-membered rings of [HGaNH]₃ connected by GaN bonds at the axial positions resolved this problem. Specifically, a hexagonal lattice can be constructed by close-packing the long cylinders parallel to one another. Use of the molecular mechanics routines available in Cerius2 allowed the minimization of the distance between the rods. The predicted lattice constant *a* for [HGaNH]_n of 7.16 Å compared well to the measured value (7.27 Å). Of equal significance was that this model provides a natural explanation for the large value of the *c* axis (32.6 Å) observed for samples of [HGaNH]_n prepared by the reaction of [H₂GaNH₂]₃ with tricyclohexylphosphine.⁷ This axis length was a direct measure of the rod length. Using the theoretical distances presented here coupled with the spacing between rods calculated using Cerius2, we estimate that a rod comprised of 11 rings, [H₃(HGaNH)₁₁H₃], would have a predicted *c* lattice constant of 32.8 Å. Samples of [HGaNH]_n prepared in liquid and supercritical ammonia exhibited a broad reflection at low angles due presumably to the presence of rods having a distribution of lengths. None of the alkylgallium analogues, [RGaNH]_n, which were all formed in supercritical ammonia, exhibited a (001) reflection that would allow assignment of the rod length. The distribution of rod lengths resulted in disorder along the *c* axis. Because this would reduce the intensity of reflections having a component along *c*, attempts to assign a cell based on the powder diffraction results were hampered. The inset graph in Figure 1 shows a plot of *d*

spacing of the (110) reflection versus the number of carbon atoms in the terminal ligand on gallium. The trend was consistent with an isostructural series that expands in size as the alkyl chain length increases.

Molecular Structure of [HGaNH]_n and [HGeCH]_n Rods. Computational methods were used to predict the detailed structure of isolated [HGaNH]_n rods and to compare them with the unknown, isoelectronic germanium carbon analogues. Structural data for the *n* = 9 case are provided in Table 5 (tabulations for all other values of *n* are provided in the Supporting Information).

There were a number of interesting trends in the data for both rods. In the GaN rod, the GaN bonds in the rings that were threaded by the rod axis became shorter as one moved from the end of the rod to the center, the net change being on the order of 0.02 Å. An opposite trend was seen in the GaN_{||} bonds, which became longer by a slightly smaller margin as one moved to the center from the ends. The combination of these trends was such that the two kinds of GaN bonds became much closer to one another in length in the center of the rod than at the ends. This suggests that the “edge effects” of the hydrogenic capping on the GaN bond lengths were not trivial. This effect manifested itself to a much lesser degree in the bond angles of the rings threaded by the rod axis. Angles at N increased by about 1° as one moved from the ends to the center, discounting the angles in the bottommost ring, where the N atoms bear two protons. Finally, H···H interatomic distances between equatorially disposed hydrogen atoms on adjacent rings that are “pointing at one another” were also tabulated (these H atoms are also the “flagpole” hydrogens for the six-membered rings in the boat conformation that form the “walls” of the rods). The distance between these atoms was about 2.6 Å. This was outside of van der Waals contact and well outside the typical range (1.7–1.8 Å) of hydride proton H–H hydrogen bonds.¹⁸ Inspection of geometries optimized at the B3LYP/CEP level for some of the shorter rods (data in Supporting Information) suggested that the MB basis set probably overestimated this distance by 0.1–0.2 Å, but that still suggested only weak electrostatic interactions between these H atoms.

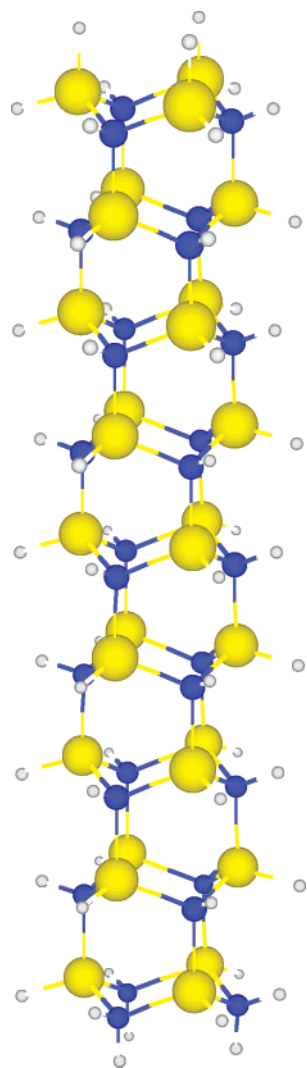
In the GeC rod, there was much less sensitivity of the geometric parameters to edge effects. GeC bond lengths remained essentially constant irrespective of position within the rod, with the GeC_{||} bonds being slightly longer than the GeC bonds in the rings threaded by the rod axis. Bond angles were also insensitive to position, as were H···H interatomic distances between rings. The latter distances were slightly longer than those in the GaN rods (about 2.8 Å), again, outside of the range that would be expected to generate any significant interaction. The most noteworthy difference between the two rods was the large difference in valence bond angles at Ga and N in the rings threaded by the rod axis compared to those of Ge and C. The former difference was on the order of 14°, while in the latter case, it was about 3°. This was rationalized by Bent’s rule.³⁴

Energetics of Rod Elongation. It was not obvious that any particularly meaningful comparison could be made between the absolute energies of the GaN and GeC rods. A more interesting prospect, however, was to examine whether there was any cooperation associated with rod elongation. That is, did the energy associated with grafting an additional ring onto a growing

(33) Luo, B.; Gladfelter, W. L. *J. Organomet. Chem.* **2004**, *689*, 666.

(34) Bent, H. A. *Chem. Rev.* **1961**, *61*, 275.

Table 5. Select Computed C_{3v} Symmetry-Unique B3LYP/MB Bond Lengths (Å) and Angles (deg) for $H_3[(HXYH)_3]_nH_3$, XY = GaN, GeC^a



Ga–N	Ga–N ^b	Ga–N–Ga	N–Ga–N	H···H
1.997	1.954	113.4	99.0	2.528
1.983	1.961	113.9	99.7	2.638
1.980	1.964	114.2	100.0	2.646
1.979	1.966	114.4	100.1	2.652
1.978	1.966	114.5	100.2	2.654
1.979	1.964	114.5	100.1	2.652
1.981	1.961	114.5	100.0	2.611
1.989	1.951	114.0	100.6	2.576
1.993		118.7	101.6	
Ge–C	Ge–C ^b	Ge–C–Ge	C–Ge–C	H···H
2.038	2.055	109.7	106.6	2.772
2.039	2.055	109.2	105.9	2.780
2.038	2.054	108.9	105.9	2.788
2.038	2.054	108.9	105.9	2.787
2.038	2.054	108.9	105.8	2.787
2.038	2.054	108.9	105.8	2.787
2.038	2.055	108.9	105.8	2.770
2.040	2.050	108.7	106.4	2.775
2.037		110.0	107.3	

^a First table row refers to the top ring, the second row to the second ring, etc. ^b X–Y_{||} indicates Ga–N or Ge–C bonds that are parallel to the rod axis.

rod become more favorable as the rod grew longer? We assessed this by evaluating the energy change associated with rod growth

Table 6. B3LYP/CEP*/B3LYP/MB Rod Growth Energetics (kcal mol⁻¹) from eq 5

n	ΔE_n	
	GaN	GeC
2	2.2	33.0
3	-4.3	32.1
4	-3.8	31.5
5	-5.2	32.0
6	-6.2	31.3
7	-7.1	32.1
8	-7.6	31.2
9	-8.3	32.3

which was, after taking account of 3 equiv of H₂, required to balance the equation where $n = 2, 3, 4, \dots$

$$\Delta E_n = E\{H_3[(HXYH)_3]_nH_3\} + E[3H_2] - E\{H_3[(HXYH)_3]_{n-1}H_3\} - E\{H_3[(HXYH)_3]H_3\} \quad (5)$$

Values for eq 5 from B3LYP/CEP*/B3LYP/MB calculations are provided in Table 6. After $n = 2$, growth of the GaN rod was predicted to be exoergic, while growth of the GeC rod was endoergic for all values of n . Moreover, growth of the GaN rod became *increasingly* exoergic with increasing n , while the endoergicity for growth of the GeC rod was effectively constant at about 32 kcal mol⁻¹.

The absolute magnitudes of the ΔE values, in general, were dictated primarily by the relative strengths of the bonds being made and broken. Two possible explanations of the origin of the increased favorability of adding new rings to the growing GaN rod compared to the GeC analogue are worth considering. First, there may be some long-range interactions present in the GaN rods that are not found for GeC, for example, a stabilizing σ delocalization. The existence of such a phenomenon would be consistent with the variations in GaN bond lengths as one proceeds from the ends of the rods (where delocalization would be expected to be reduced) to the center (where it would be maximal). However, it was difficult to provide a more convincing demonstration of such an effect.

An alternative explanation for the increasing favorability of rod growth is to note that the electric dipole moment of the GaN rod, as discussed in more detail below, grew substantially with each additional ring. A new ring, even if the intervening H atoms present prior to it being grafted onto the rod were removed, had an electric dipole moment exactly aligned (end-on) with the rod's. Thus, there was an electrostatic driving force for each new ring attachment that would be expected to grow roughly linearly with each new ring.

One difference between these two possibilities was that the delocalization phenomenon might be expected to saturate once the rod exceeds the optimal delocalization length. In that case, additional rings would be expected to add with favorable attachment energies, but that energy would reach some plateau. The dipole–dipole effect, on the other hand, would *not* be expected to saturate since the rod's dipole moment increases with each additional ring (vide infra). Inspection of the data in Table 6 does not suggest that any plateau has been reached by $n = 9$. This could either mean that the dipole–dipole effect was dominant, that the delocalization length was longer than 9 (which seemed intuitively unlikely, but could not be ruled out), or that the delocalization effect, if it existed, did not saturate.

Table 7. B3LYP/CEP*/B3LYP/MB Electric Dipole Moments (D) of $H_3[(HXYH)_3]_nH_3$, $n = 1-9$, XY = GaN, GeC

n	Dipole Moment	
	GaN	GeC
1	2.7	1.0
2	9.0	1.1
3	15.5	0.9
4	23.0	0.5
5	31.3	0.1
6	40.3	-0.4
7	49.7	-0.9
8	59.4	-1.5
9	69.3	-2.1

We considered the electrostatic explanation to be the most reasonable based on arguments outlined in more detail below, but the computational data did not permit an especially firm conclusion to be made. In any case, the lack of any cooperation in the growth of the GeC rod was consistent both with a lack of any special delocalization energy and with the very small rod dipole moments discussed below.

Rod Electronic Structures. A particularly noteworthy difference between the GaN and GeC rods was the extent of charge separation intrinsic to the former but absent in the latter. The first nonvanishing electrical moment in these systems, the dipole moment, quantified this difference (Table 7). As the rods had an axis of symmetry, their dipole moments lay along their axes. In the GaN rods, the dipole moments were seen to increase monotonically by 6–10 D with each additional ring, such that by the time $n = 9$ was reached, the dipole moment was a striking 69.3 D.

This behavior was easily rationalized. The constituent cyclotrigallazane rings were themselves quite polar. If one viewed these rings, in the limit, as a plane of gallate anions positioned above a plane of ammonium cations, then it was easy to rationalize the sign of the dipole moment (the orientation we employed for all analyses of rod dipole moments placed the plane of capped heavy atoms above and the plane of capped light atoms below; a positive dipole moment implied buildup of negative charge on the heavy atom end, and a negative dipole moment implied the opposite). This significant separation of charge in the parent ring was amplified by rod extension; one may consider the connection of the new ring to the growing rod as annihilating the charges being connected and ultimately increasing the distance between the charged capping fragments. Of course, this view of formally charged capping fragments overstated the situation; a full separation of three charge units over the length of the $n = 9$ GaN rod would correspond to a dipole moment of 298.4 D, but it provided a qualitatively informative representation of the electronic polarization.

The GeC rods, on the other hand, exhibited at first inspection rather curious behavior. The dipole moment of the parent ring was +1.0, but rod extension slowly reduced the dipole moment until it passed through zero and then became increasingly negative. The explanation for this behavior reflected the fundamental difference between a group 13/15 system and a group 14/14 system. While the former had a nontrivial degree of ionicity, the latter had almost none. Thus, in the heavy-atom framework of the 1,3,5-trigermacyclohexane, we expected the less electronegative Ge atoms to pass negative charge to the more electronegative carbon atoms, which corresponded to a negative dipole moment if the heavy atoms were above the light

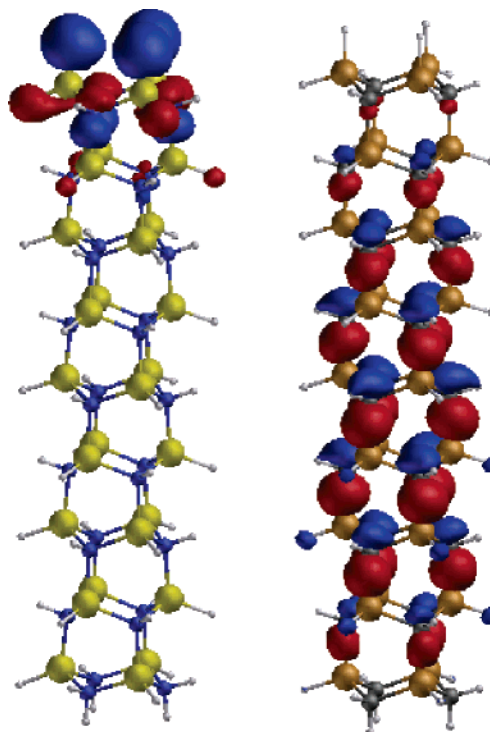


Figure 6. Highest occupied molecular orbitals (HOMOs) from the a_1 irreducible representation for rods $H_3[(HXYH)_3]_9H_3$, XY = GaN (left) and GeC (right), at the B3LYP/CEP*/B3LYP/MB level.

ones (in the positive z -axis direction). Stacking an increasing number of such rings one atop another would be expected to amplify this effect, and that was ultimately what was seen in the longest rods, although the small difference in electronegativities between Ge and C made the incremental effect only about 0.6 D in magnitude per ring.

What then accounted for the positive dipole moments in the monomer and shorter rods? It was the combined influence of the axial C–H and Ge–H bonds. These bonds lie along the dipole moment axis, so their effect on the moment was maximized. Moreover, the orientation of these bonds was such that the less electronegative atom was always at the bottom and the more electronegative at the top. Thus, they contributed to a positive dipole moment, and this effect outweighed the initially small negative dipole moments associated with the heavy-atom framework. However, since the number of these axial bonds was constant, three of each in every rod, their influence is eventually overwhelmed by the cumulative dipole moments of the framework rings, and the net moment became negative after $n = 5$.

The differential polarizations, both in sign and in magnitude, of the GaN and GeC rods had interesting effects on the spatial properties of the molecular orbitals in these systems. Orbitals of particular interest in the rods were those belonging to the a_1 and a_2 irreducible representations (irreps) of the C_{3v} point group as their axial symmetry rendered their interpretation particularly facile. Shown in Figures 6 and 7 are the highest occupied MOs from each of these two irreps, respectively, for each rod. The a_1 irrep contained MOs derived from combinations of bonding and/or antibonding orbitals for the $XY_{||}$ bonds (as well as potentially the axial XH and YH bonds), while the a_2 irrep contained MOs derived from combinations of bonding and/or

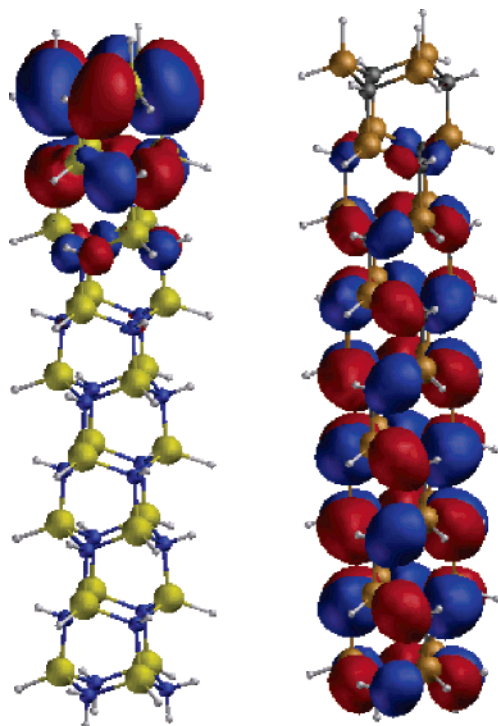


Figure 7. Highest occupied molecular orbitals (HOMOs) from the a_2 irreducible representation for rods $H_3[(HXYH)_3]_nH_3$, XY = GaN (left) and GeC (right), at the B3LYP/CEP*/B3LYP/MB level.

antibonding orbitals for the XY bonds in the rings threaded by the rod symmetry axis.

One canonical model for the sets of MOs in these irreps would be that they would begin with a lowest energy orbital delocalized over the entire length of the rod and having zero nodes; the next higher such orbital in energy would have one node, the next higher after that would be two, etc., until one reached the highest energy such orbital (a virtual orbital) that would have $N - 1$ nodes, where N is the number of framework atoms. This model in fact served as a reasonable description of the relevant GeC MOs, although we do not show here the orbitals other than the HOMOs within each irrep (which have $(N/2) - 1$ nodes). They were fairly well delocalized along most of the rod and strikingly symmetric in appearance.

The same cannot be said for the GaN rods, however, where the corresponding HOMOs were highly localized near the Ga capping layer. The GaN rods followed a different orbital hybridization model. In essence, the substantial rod dipole moment acted as a strong perturbation on the electronic Hamiltonian operator. So, rather than orbitals preferring to be delocalized with relative energy depending on the number of nodes, orbitals in the GaN rod preferred to be localized, with energy depending first on the distance from the positive end of the rod dipole, and second on the bonding or antibonding characteristics of the constituent local bond orbitals. Thus, although again the orbitals are not shown, the lowest energy MO within each irrep was a bonding-type MO highly localized near the nitrogen capping layer, the next highest energy orbital was one step higher on the rod, and so on. By the time the HOMO was reached, the MO was localized at the negative end of the rod, but still involved bonding-type local bond orbitals. In the virtual manifold, the orbitals returned to being closer to the positive end of the dipole, but increasingly contained σ -antibonding components.

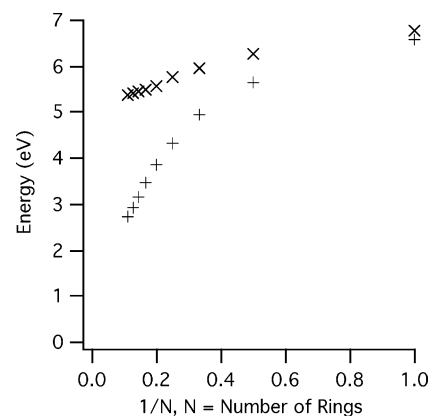


Figure 8. Excited-state energies relative to the ground state (eV) for the lowest excited states of $H_3[(HXYH)_3]_nH_3$, XY = GaN (+), GeC (x); $n = 1-9$ calculated at the TD-B3LYP/CEP* level and plotted against $1/n$.

Returning to the GeC rods with a somewhat closer inspection, we found that the dipolar influence noted for GaN did exist in the GeC systems, it was just that it was manifested to a much lesser degree. Thus, although the orbitals in Figures 6 and 7 were highly delocalized, they were slightly polarized toward the “down” side of the rod, consistent with the reversed sign of the dipole moment in the GeC rods compared to the GaN ones.

Rod Electronic Excitation Energies. The different behaviors of the rod dipole moments upon rod elongation also significantly affected the energy separations between the electronic ground state and the lowest energy excited states (the “band gap” for these rather small solid systems, one might aver). Computed at the TD-B3LYP/CEP*/B3LYP/MB level and plotted against an effective inverse rod length (Figure 8), one sees that the GeC excitation energies were only weakly influenced by rod length, and that the rod was a fairly strong insulator, with a gap in excess of 5 eV predicted from extrapolation of this plot to zero on the abscissa (corresponding to $n = \infty$). The GaN excitation energies, on the other hand, started near those of the small GeC systems, but rapidly dropped with increasing rod length. To the extent that these excitations may be viewed as involving intramolecular charge transfer from the negative end of the rod dipole to the positive end, this was exactly the behavior one would expect as the rod dipole grows larger. Extrapolated to infinite rod length, the TD-B3LYP calculations predicted a band gap of about 1.5 eV, which is near the red end of the visible spectrum. Of course, these pseudo-one-dimensional rods (which may still contain substantial end effects at $n = 9$) cannot be taken to be accurate representations of crystalline gallium nitride (which has an experimental band gap of 3.4 eV), but the computational results were provocative in terms of highlighting the electronic structure differences between the group 13/15 rod and its group 14/14 analogue. The impact of surface capping ligands on optical properties was recognized in the study of cadmium selenide clusters stabilized by selenophenoxide.⁶

Known molecular clusters with framework gallium and nitrogen atoms were substantially smaller than the rod structures reported here, typically colorless, and were not known to emit light. On the basis of the calculations described above, the low-lying excited states for the $[R\text{GaNH}]_n$ rods arose from an intrarod charge transfer and even for relatively small rods were expected to absorb in the near-ultraviolet region. The calculated energies of the excited states decreased as the rod length increased, and we propose that the structure observed in the

fluorescence spectra of **1** and **2** resulted from emission from rods of differing lengths. The observation that degradation in air affected the emission intensity of some emission peaks more rapidly than others was consistent with an assignment of each emission peak to a unique compound. The synthetic procedures were expected to produce a distribution of rod sizes.

The emission maxima in **1** occurred at 2.87, 2.73, and 2.58 eV. Assuming a similar Stokes shift for rods of different length, we compared the energy difference among these peaks to the calculated energy gaps. Note that for rods having $n > 9$, the energy versus rod length was determined by extrapolation of the trend calculated for smaller rods. Thus, the observed gaps of 0.134 and 0.127 eV corresponded to the energy difference of 0.134 and 0.115 eV estimated for $H_3[(HGaNH)_3]_{10}H_3$, $H_3[(HGaNH)_3]_{11}H_3$, and $H_3[(HGaNH)_3]_{12}H_3$. The predicted absolute energy for absorbance for these rods is 2.60, 2.47, and 2.35 eV, approximately 1 eV lower than the experimental absorption energy centered around 316 nm. Clearly, there were several assumptions that were required for this analysis, and more research is needed to quantify the relationships. A similar analysis of the emission peaks for **2** at 3.18, 2.94, 2.73, and 2.55 eV found similar energy gaps that suggested similar size rods. The most intense emission peak may have resulted from a larger proportion of smaller rods in the distribution.

It is interesting to compare these molecular level oligomers to the nanorods and wires of GaN that are of great current interest.^{35–38} The radius of the GaN core in $[RGaNH]_n$ is 0.3 nm compared to that of 4 nm for the smallest nanorods. Consistent with the larger size, the optical properties of the nanorods are similar to those of bulk GaN.

Conclusions

Ammonolysis of $[RGa(NMe_2)_2]_2$ led to microcrystalline powders having the general formula of $[RGaNH]_n$. X-ray powder diffraction and crystal structure modeling established that stacks of six-membered $[RGaNH]_3$ rings connected through

axial Ga–N bonds comprised the rod cores, which were coated with a hydrocarbon shell. Rod length was not determined for the alkyl gallium compounds, but reanalysis of the diffraction data for $[HGaNH]_n$ was consistent with a long axis of 32.8 Å that corresponded to 11 stacked $[HGaNH]_3$ rings.

Comparison of the electronic structures of the more polar Ga–N rods to those of the isoelectronic Ge–C rods suggested that large and increasing electric dipole was responsible for the increasing stability of rods of increasing length for the Ga–N case, while no cooperative effect was observed in the Ge–C case. In another contrast between the two kinds of rods, σ framework molecular orbitals were highly delocalized in the Ge–C case, but the large dipole moments in the Ga–N rods caused the corresponding molecular orbitals to be much more localized. In particular, the Ga–N HOMO involved bonding orbitals localized at the negative end of the GaN rod, while the low-lying virtual orbitals exhibited localization toward the positive end. Thus, low-lying excited states may be thought of as involving dipole-assisted intramolecular charge transfer. This phenomenon caused the HOMO–LUMO gap to decrease significantly as a function of Ga–N rod length, which was in contrast with a roughly constant gap predicted for the Ge–C system. Experimental photoluminescence spectra for Ga–N samples exhibited distinct emission peaks with energetic separations consistent with those predicted by theory for absorption by rods of differing integral lengths.

Acknowledgment. The authors gratefully acknowledge support from the National Science Foundation (W.L.G., CHE-03159540; C.J.C., CHE-0203346). We thank Professor S. Lipsky for the use of his spectrofluorometer and for valuable discussions.

Supporting Information Available: X-ray crystallographic files in CIF format for the structure determinations of compounds **1** and **9**. Select structural data for computational oligomers of length 1–8 at all applied levels of theory. This material is available free of charge via the Internet at <http://pubs.acs.org>.

JA045149F

- (35) Han, W.; Fan, S.; Li, Q.; Hu, Y. *Science* **1997**, *277*, 1287.
(36) Duan, X.; Lieber, C. M. *J. Am. Chem. Soc.* **2000**, *122*, 188.
(37) Chen, C.-C.; Yeh, C.-C.; Chen, C.-H.; Yu, M.-Y.; Liu, H.-L.; Wu, J.-J.; Chen, K.-H.; Chen, L.-C.; Peng, J.-Y.; Chen, Y.-F. *J. Am. Chem. Soc.* **2001**, *123*, 2791.
(38) Huang, Y.; Duan, X.; Cui, Y.; Lieber, C. M. *Nano Lett.* **2002**, *2*, 101.